

Holocene summer temperature reconstruction from sedimentary chlorophyll content, with treatment of age uncertainties, Kurupa Lake, Arctic Alaska

The Holocene
2015, Vol. 25(4) 641–650
© The Author(s) 2015
Reprints and permissions:
sagepub.co.uk/journalsPermissions.nav
DOI: 10.1177/0959683614565929
hol.sagepub.com


Brandon R Boldt,¹ Darrell S Kaufman,¹ Nicholas P McKay¹
and Jason P Briner²

Abstract

Quantitative records of pre-industrial temperature changes are fundamental for understanding long-term natural climate variability. We used visible reflectance spectroscopy to measure chlorophyll content (and its derivatives) in a sediment core from Kurupa Lake, north-central Brooks Range, Alaska, to reconstruct summer temperature and the number of annual non-freezing days over the past 5.7 ka. A calibration-in-time approach was used to convert downcore changes in chlorophyll content to the climate variables, and an ensemble approach was used to integrate age and calibration uncertainties. The strongest correlation ($r_{\text{median}}=0.69$, $p_{\text{median}}=0.02$, RMSEP=1.9°C) is for summer (June through September) temperature using the 20th Century Reanalysis Project dataset. The chlorophyll-inferred 3-year-mean summer temperature shows that the warmest century (3.0–2.9 ka BP) was about 3.0°C (90% range of the ensemble members=2.3–4.0°C) higher and that the coldest century (1.4–1.3 ka BP) was about 5.5°C lower (90% range=–7.6°C to –5.0°C) than during the reference period (AD 1961–1990). Century-to-century temperature changes over the past 5.7 ka at Kurupa Lake have been large (90% range=–2.8°C to 3.1°C shifts in centennial mean), including the shift between the 19th and 20th centuries, which was above the 90th percentile of temperature changes across all representations of the reconstruction. In contrast to most Northern Hemisphere temperature reconstructions, Kurupa Lake shows no overall millennial-scale cooling trend. We suggest that increased summer duration (by 4.3 days during the last 6 ka) along with no long-term increase in sea-ice cover over the adjacent Chukchi Sea counter-balanced the influence of decreased insolation intensity on the aquatic productivity in Kurupa Lake.

Keywords

age uncertainty, Brooks Range, Holocene, lake sediment, paleoclimate, proxy-climate record

Received 29 November 2014; revised manuscript accepted 30 November 2014

Introduction

Changes in the sea-ice cover of the Arctic Ocean are known to have a major effect on air surface temperatures (e.g. Walsh et al., 2011). Considerable progress has been made recently to reconstruct Arctic sea-ice conditions during the Holocene (e.g. Polyak et al., 2010), but less work has focused on linking these changes to Holocene climate changes represented by terrestrial records. The high amplitude of variations in the sea-ice cover over the Chukchi Sea during the Holocene (de Vernal et al., 2013) and during the 20th century (e.g. Walsh and Chapman, 2001) indicate that this region, which is close to the present-day winter sea-ice margin, is highly sensitive to climatic changes. Few high-resolution proxy climate records have been developed for the region, but are needed to investigate the impacts of sea-ice changes on terrestrial conditions of the Arctic Ocean borderlands.

Seasonally ice-covered Arctic lakes are sensitive to minor changes in climate that influence the length of the short growing season (Smol, 1988), and these changes are represented by a variety of sedimentary proxy-climate indicators (cf. Sundqvist et al., 2014). Variability in chlorophyll content of lake sediments is mainly related to autochthonous primary production (Das et al., 2005; Michelutti et al., 2005, 2010). Chlorophyll content of

sediment can be measured at sub-centimeter scale with rapid and non-destructive visible reflectance spectroscopy. Previous research shows good agreement between spectrally inferred and conventionally measured chlorophyll concentrations (Das et al., 2005; Michelutti et al., 2005, 2010; Wolfe et al., 2006), and shows that reflectance-based sedimentary chlorophyll content can be correlated with instrumental records of climate (von Gunten et al., 2009; Saunders et al., 2013).

In this study, we reconstructed summer temperature at Kurupa Lake, which is situated along the northern flank of the Brooks Range, Alaska, and separated from the coast of the Chukchi Sea

¹School of Earth Sciences and Environmental Sustainability, Northern Arizona University, USA

²Department of Geology, University at Buffalo, USA

Corresponding author:

Darrell S Kaufman, School of Earth Sciences and Environmental Sustainability, Northern Arizona University, 625 S Knoles Dr, Flagstaff, AZ 86011-4099, USA.

Email: darrell.kaufman@nau.edu

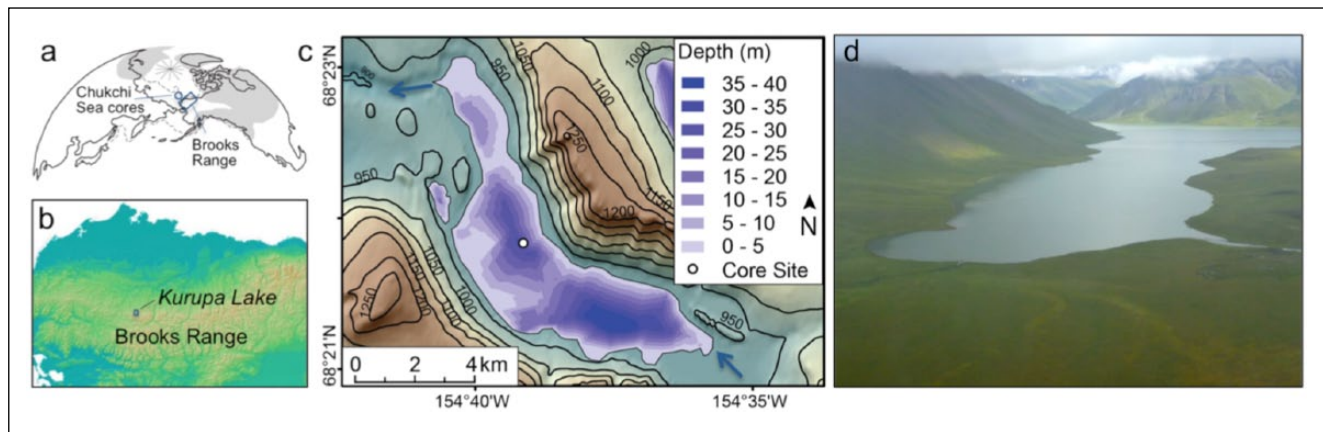


Figure 1. Location of Kurupa Lake in the context of (a) the Northern Hemisphere, showing the rough extent of ice sheets during the global 'Last Glacial Maximum' (gray area) and the continental shelf break (dashed lines), and (b) northern Alaska. (c) Kurupa Lake bathymetry and topography of adjacent area (contours in meters), with core site indicated by white circle. Blue arrows mark the primary inflow and outflow. (d) Kurupa Lake looking upvalley (to the southeast), with the outflow in lower right.

by the broad, low-laying Arctic coastal plain (Figure 1). Past temperature fluctuations were inferred based on changes in primary production as represented in the lacustrine sediment sequence, which extends back to 5.7 ka. We used the calibration-in-time approach to proxy calibration (see von Gunten et al. (2012) for a recent review) to develop the relation between regional climate and spectrally inferred chlorophyll and its degradation products (herein referred to simply as 'chlorophyll') in the sediments of Kurupa Lake. The basic procedure was to compare sedimentary spectral indices with instrumental climate data during the period of overlapping observations, and to produce a regression-based linear predictive model for changes in temperature. This lake-specific inference model was then applied to downcore spectra (proxy series) to infer paleotemperature changes. We expanded on this approach by evaluating the influence of age uncertainty for both the calibration and its transfer downcore, as well as the importance of the choice of instrumental temperature product on the reconstructed temperatures. We then focus on metrics of the temperature reconstruction, including their uncertainties, that are well suited to comparison with climate-model simulations.

Kurupa Lake setting

Kurupa Lake (N 68.35°, W 154.61°) is a relatively large (6.5 km²), deep (z_{\max} = 40 m) lake situated at 920 m.a.s.l. at the northern front of the Brooks Range (Figure 1). The lake is fed by several tributaries, including meltwater from eight rapidly disappearing cirque glaciers. Mean annual and mean summer (JJAS) air temperature between 1961 and 1990 in the 2° grid that contains Kurupa Lake are -4.3°C and 10.3°C, respectively (Compo et al., 2011). Gridded temperature data were used because weather stations in the Brooks Range are scarce and time series are discontinuous. Nonetheless, the gridded and instrumental temperature data at Barrow (1950–2005) are highly correlated ($r=0.88$, $p<0.01$; Boldt, 2013).

The northern flank of the Brooks Range is strongly influenced by the climatic regime of the adjacent Arctic Ocean. Differential heating between the Arctic Ocean and the northern front of the Brooks Range produces continual frontal activity, which is especially pronounced during the snow-free summer (Lynch et al., 2001). Precipitation occurs due to frontal activity peaks in summer and is minimized during winter by reduced inland flow of North Pacific moisture-bearing winds that yield to high pressure over the Beaufort Sea (Stone et al., 2002). The extent of sea-ice over the Arctic Ocean, especially during the transitional seasons (average Oct + Nov + Feb + Mar of the same hydrologic year;

http://nsidc.org/data/seaice/data_summaries.html) likely influences moisture availability and precipitation, as indicated by the inverse correlation with precipitation amount at Barrow (average Oct + Nov + May + Jun; $r=-0.55$, $p=0.007$).

Materials and methods

The recovered sedimentary sequence from Kurupa Lake is a composite of a 6.2-m-long percussion core (KU10-2A) and a 0.5-m-long companion surface core (KU10-2C). Both were collected in 2010 from the primary depositor of Kurupa Lake (depth=34 m). The sediment, as described by Boldt (2013), is composed primarily of laminated (sub-millimeter to 5-cm-thick beds) clay to medium silt. The organic-matter content as determined by loss on ignition is relatively low and constant throughout, ranging from 7% to 8%. The uppermost 7 mm of sediment (2004–2010) was deformed and not considered further.

Geochronology

Six samples of organic material for radiocarbon analysis were taken from core KU10-2A (Table 1). Sediment samples between 0.5 and 2.0 cm thick were wet-sieved to isolate macrofossils. Three samples were composed of twigs and other terrestrial plant fragments. The other three samples comprised bryophytes and other aquatic plant material. Macrofossils were analyzed for ¹⁴C at the University of California, Irvine. A ²³⁹⁺²⁴⁰Pu activity profile was analyzed from the upper 12 cm of surface sediment (KU10-2C) to capture the 1963 Pu spike of Pu fallout from atmospheric weapons testing (Ketterer et al., 2004). The Pu activity of 2-mm-thick, non-contiguous samples was measured using inductively coupled plasma mass spectrometry at Northern Arizona University (Table 2). An age–depth model for the sediments of site 2 (KU10-2A and -2C) was developed using the ¹⁴C ages, the peak in Pu activity (1963), and the age of the sediment–water interface (2010). An ensemble of 10,000 age models was constructed by fitting the age–depth data with a cubic spline (type=3) using the *clam* v2.1 code (Blaauw, 2010). The routine generates Monte Carlo age–depth fits through the calibrated-age probability distributions. All ages are presented in calendar years prior to AD 1950 (cal. BP or ka BP).

Reflectance spectroscopy

We measured visible reflectance spectroscopy (360–740 nm at 10-nm resolution) on the fresh split-core face with a Konica

Table 1. Radiocarbon and calibrated ages from KU10-2.

Lab ID ^a	Depth blf (cm) ^b	¹⁴ C age (yr BP)	Calibrated age ^c	Dated material
89094	76.5	440 ± 20	506 ± 20	Bryophytes, bryophyte branches
89095	167.5	1470 ± 15	1355 ± 37	Twig
89096	224.5	2035 ± 15	1982 ± 55	Bryophytes, terrestrial large leaf fragment
88968	398.0	3315 ± 20	3530 ± 70	Terrestrial woody twig
88969	505.5	4020 ± 20	4478 ± 50	Bryophyte twig with many leaves, woody stems
84708	593.5	4665 ± 20	5401 ± 74	Tree bryophyte stems with leaves

^aKeck Carbon Cycle AMS Facility, University of California Irvine (UCIAMS).

^bCentered sample depth; samples 1.0-cm thick.

^cMedian probability ± one half of the 1σ range; calibrated using CALIB 6.0 (Stuvier et al., 2005).

Table 2. ²³⁹⁺²⁴⁰Pu profile from core KU10-2C.

Depth blf (cm) ^a	Pu activity (Bq/kg)
0.1	0.23
1.1	0.22
2.1	0.29
3.1	0.54
4.1	0.34
4.3	–
4.5	0.29
4.7	0.45
4.9	2.00
5.1	1.11
5.3	2.00
5.5	5.60
5.7	6.38
5.9	5.22
6.1	3.50
7.1	0.11
8.1	0.00
9.1	0.00
10.1	0.00
11.1	0.00

^aDepths are mid-points of 2-mm-thick samples.

Minolta CM-2600d spectrometer at 2-mm intervals, corresponding to about 2 years of sedimentation. Analyses were performed at the Limnological Research Center, University of Minnesota. The relative absorption-band depth between 660 and 670 nm (RABD_{660;670}, hereafter, ‘RABD’) was used to quantify total sedimentary chlorophyll and its diagenetic products, which have absorption maxima between 660 and 690 nm (Wolfe et al., 2006). RABD is defined as the ratio between the reflectance minimum (absorption maximum) and the reflectance value for the same wavelength, assuming a linearly interpolated reflectance continuum. Following Rein and Sirocko (2002), RABD is calculated as:

$$\left[\left(6 * R_{590} + 7 * R_{730} \right) / 13 \right] / R_{\min(660;670)} \quad (1)$$

where R₅₉₀=reflectance at 590 nm, R₇₃₀=reflectance at 730 nm, R_{min(660;670)}=minimum reflectance at 660 or 670 nm.

Treatment of uncertainties

Calibration uncertainty

The spectral parameter (RABD) and climate time series (AD 1871–2003) were resampled by binning both datasets in 3-year intervals. Total least-squares regressions were calculated between the proxy data and instrumental time series. Age uncertainty of the proxy data over the instrumental period was incorporated into the

analysis by iterating the regression using 1000 members of the age-model ensemble from the *clam* output. In addition, regression stability was addressed using a jackknife procedure. To assess the impact of age uncertainty and the sensitivity of the regression to individual 3-year-temperature-RABD pairs, we calculated 1000 ensembles of the temperature reconstruction by randomly selecting an age-model ensemble, and removing one of the 3-year-mean calibration intervals for each member. These reconstructed temperature ensembles were then used to estimate uncertainties associated with the least-squares regression coefficients (slope, intercept, and *r*-value; calculated as the 1σ range of the members). The cross-validated root-mean-squared error of prediction (RMSEP) was also calculated for all ensemble members. This process was performed using two temperature reanalysis products and one estimate of the number of above-freezing days (see below).

Reconstruction uncertainty

RABD was modeled as a function of temperature (or above-freezing days) using total least-squares regression. The influence of age uncertainty on the reconstruction was evaluated by applying the calibration equation to each of 1000 members of the age-model ensemble from the *clam* output. Similarly, Bakke et al. (2013) used the multiple age–depth models from *clam* to integrate the uncertainty in age control into uncertainty in the proxy record. Here, we expanded on this approach by applying a different calibration equation for each iteration. The median and 1σ and 2σ ranges of the reconstructions were determined from the large ensemble of plausible reconstructions. This illustrates the sensitivity of the reconstructions to age uncertainty and regression stability as described above (including the impact of age uncertainty on the regressions), but does not consider additional sources of uncertainty (most notably the assumption of stationarity), and the ensemble spread does not represent a formal estimate of temperature probability.

Choice of instrumental dataset

The confidence intervals for the reconstructions integrate the uncertainty in both the geochronology and the regression statistics used for proxy calibration. They do not, however, include the errors inherent in the instrumental temperature records used for calibration. Three different reanalysis products were considered to assess how the choice of instrumental data influenced the reconstructions. We extracted the summer (JJAS) temperature data from the grid cell nearest to Kurupa Lake in the: (1) 20th Century Reanalysis Project, hereafter ‘20CR’ (Compo et al., 2011), which is based on an assimilation of surface pressure and uses sea-surface temperature and sea-ice distributions as boundary conditions, and two products that integrate air and sea-surface temperature measurements: (2) NASA’s GISTEMP (Hansen et al., 2010) and (3) Hadley Centre’s HadCRUT4 (Morice et al., 2012). We also calculated the number of days above freezing for

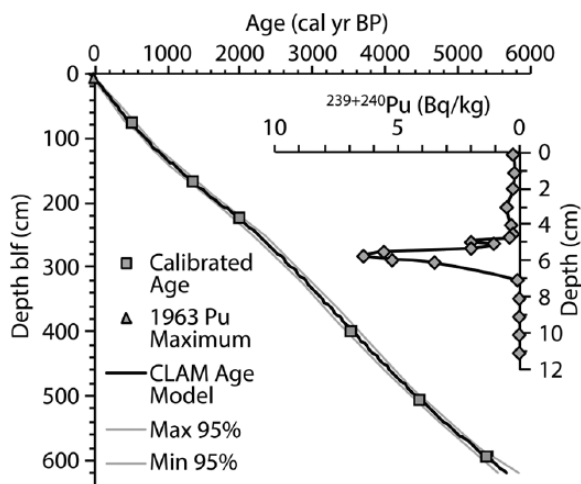


Figure 2. Age–depth model for Kurupa Lake site 2 composite core. Radiocarbon ages were calibrated to calendar years prior to AD 1950 (cal yr BP) and a smoothed cubic-spline function was used to model the age–depth relation and 95% confidence intervals with clam v2.1 according to the methods of Blaauw (2010). Inset shows $^{239+240}\text{Pu}$ activity profile with peak at 5.7-cm depth assigned to 1963. Radiocarbon data are listed in Table 1, and Pu data are in Table 2.

each year using six-hourly temperatures from the 20CR as an indicator of the length of the growing season.

Results and discussion

Geochronology and RABD

Downcore changes in $^{239+240}\text{Pu}$ activity in the surface core from Kurupa Lake (KU10-2C) show a well-defined peak at 57-mm depth (Figure 2, inset), which we assigned to AD 1963. The sedimentation rate is nearly linear down to the onset of Pu activity (AD 1953) at 71 mm. On the basis of our age model (Figure 2), the sedimentation rate (0.9–1.3 mm/yr) is relatively constant throughout the sedimentary sequence. The 95% confidence intervals increase from ± 2 years at the core top to ± 23 years at AD 1871, the start (base) of calibration period. The age-model uncertainty averages ± 52 years over the 5722-year-long core, as evaluated every 2 mm, the spacing of the proxy data.

Downcore changes in RABD values show coherent fluctuations on decimeter to meter scales (Figure 3), corresponding to centennial to millennial time scales. RABD values of sediment deposited during the instrumental period encompass nearly the entire range of variability over the full record. Specifically, only 5% of the values are lower than the value for 1898 and none are higher than for 2003.

Proxy calibration

Total least-squares regressions were calculated between the RABD and instrumental time series using an ensemble approach to integrate uncertainties in ages and regression stability (Figures 4 and S1, available online). Of the three reanalysis products, RABD is most strongly correlated with summer (JJAS) temperature data from 20CR ($r_{\text{median}} = 0.69$, $p_{\text{median}} = 0.02$, $\text{RMSEP}_{\text{median}} = 1.9^\circ\text{C}$), with more than 83% of the ensemble-member correlations significant at the $\alpha = 0.05$ level (p -values were corrected to account for lag-1 autocorrelation according to Bretherton et al. (1999)). The number of days per year with above-freezing temperature from 20CR also correlates strongly with RABD, consistent with the hypothesized mechanism for the response of organic production to changes in temperature. Strong relations were also found for JJAS temperatures from GISTEMP. In contrast, correlations using the

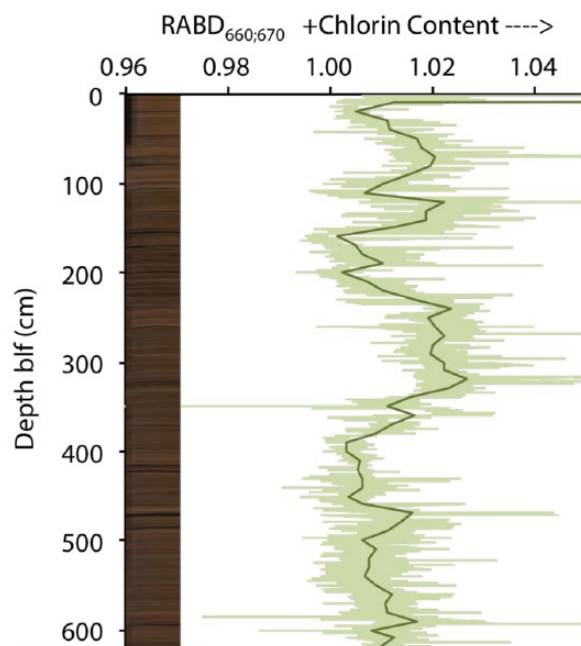


Figure 3. Line-scan image of sedimentary sequence from Kurupa Lake site 2, RABD_{660,670} (chlorophyll content). Light green curve shows 0.2-cm resolution; dark curve is smoothed with linear integration to 10-cm interval.

HadCRUT4 reanalysis product are not significant, and are not considered further. This probably reflects the absence of spatial interpolation to account for the incomplete data coverage over regions void of data, including the Arctic.

Although the uncertainty analysis considers a range of temperature–RABD relations, it does not explicitly account for the possibility that the relation between temperature and pigment concentration has changed through time (i.e. non-stationarity). Numerous variables, both internal and external to Kurupa Lake, can affect primary production and photosynthetic pigment preservation following deposition. For example, the rate of chlorophyll production could depend on changes in the community structure of primary producers. Landscape and vegetation change, increased loess transport, and re-suspension of sediment within the lake can increase nutrients and stimulate aquatic primary production.

Stationarity cannot be guaranteed; however, we suggest that the primary processes that govern chlorophyll content at Kurupa Lake have been relatively uniform for millennia. The lake has a large surface area (6.5 km²) and depth (40 m), which suggests greater stability compared with smaller lakes during periods of modest climate change; lake level and stratification of large, deep lakes are less variable in response to change in evaporation/precipitation compared with small, shallow lakes. Long-term uniformity can be inferred from the relatively constant sedimentation rate and lack of major sedimentological changes. Continuous laminations (<1 mm to cm scale) suggest suboxic to anoxic benthic conditions for the past 5.7 ka, with little degradation of organic matter, and therefore little time-averaging of the sediment. There is no long-term trend in RABD prior to the calibration period (Figure 3). Michelutti et al. (2010) recognized similar tendencies in multiple sediment cores and confirmed that spectrally inferred measurements of chlorophyll track past changes in aquatic primary production rather than photosynthetic pigment degradation through time. Finally, the modern distribution of vegetation communities in the northern Brooks Range was achieved between 6 and 4 ka (Anderson and Brubaker, 1994), suggesting that major vegetation shifts have not occurred during most of our record.

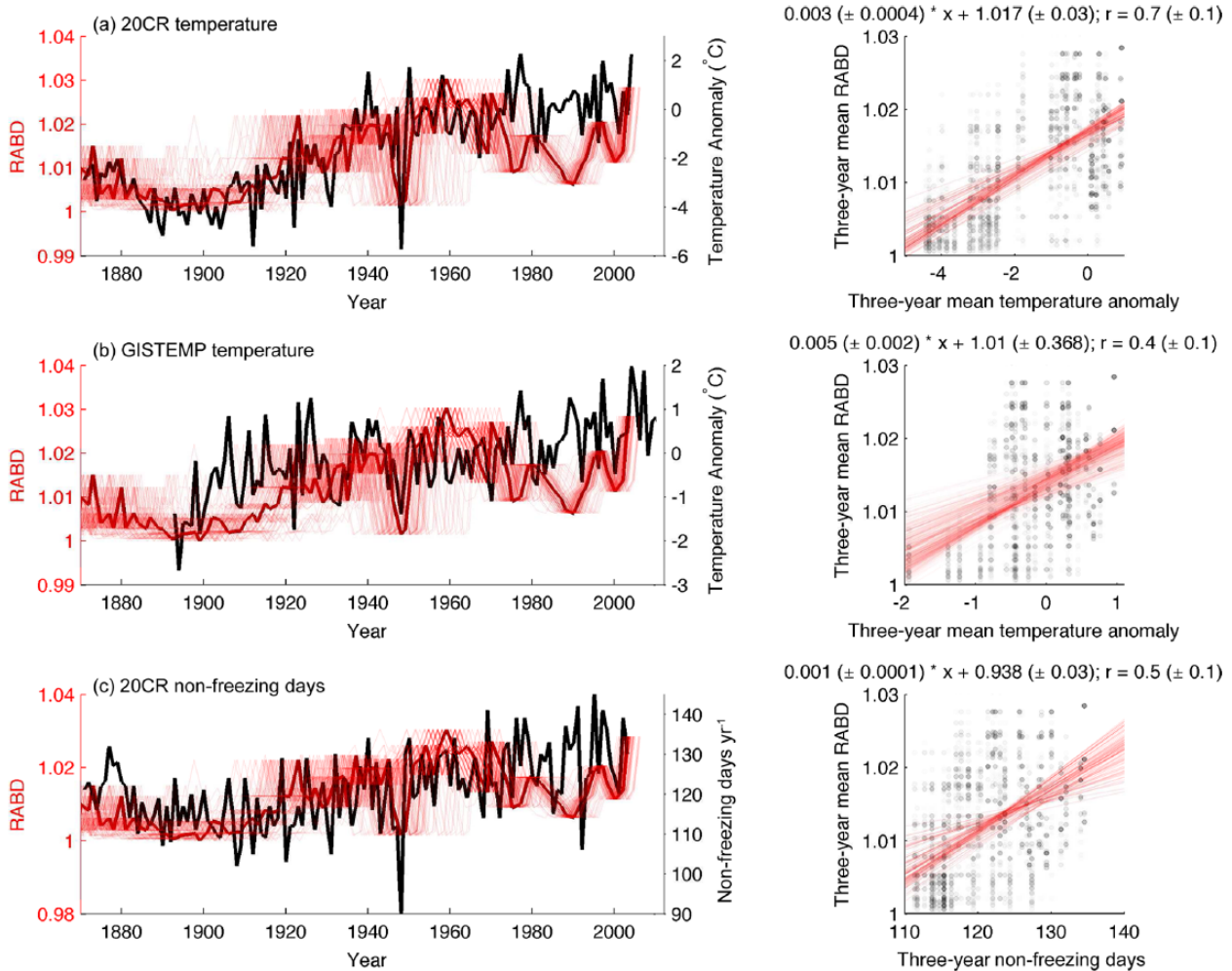


Figure 4. Relative absorption-band depth (RABD) from Kurupa Lake sediment and instrumental climate data for 1870–2010 based on reanalysis products. Reference period is AD 1961–1990. Left panels: JJAS temperature from the grid cell nearest Kurupa Lake (black) from the 20th Century Reanalysis Project (top row; Compo et al., 2011), GISTEMP (middle; Hansen et al., 2010), and the number of days per year with an average temperature above freezing (bottom; Compo et al., 2011). The fine red lines are the RABD plotted with different members of the age-model ensemble, illustrating the effect of time uncertainty; the bold red line shows RABD plotted with the best-estimate age model. Right panels: scatterplots of 3-year-mean reanalysis and RABD data, including the effect of age uncertainty. A total of 10,000 points sampled from the different age ensemble members are plotted as gray dots whose opacity is proportional to the frequency of occurrence across age-model ensembles. Fine red lines show the regressions calculated for different age ensemble members. The median and one standard deviation of the regression statistics are listed above each panel and were propagated into the reconstruction step.

Holocene summer temperature (and non-freezing-days) reconstructions and uncertainties

Downcore 3-year-mean RABD values from Kurupa Lake were converted to JJAS temperatures using the total least-squares regression models (Figure 5). The models integrate the uncertainty due to both age and calibration uncertainty by using an ensemble dataset in which 1000 constituent members sample the multiple sources of uncertainty and propagate them through to the reconstruction (Figure S1, available online). Most of the uncertainty is associated with the calibration (age uncertainty and regression robustness), which impacts the amplitude of the temperature reconstruction. Less of the overall uncertainty is ascribed to the age-model downcore, which influences the extent to which the median-ensemble time series is smoothed. The weighted mean of the probability distribution for each 3-year time slice from all ensemble members was used for the final reconstruction, and is necessarily smoother than each constituent member (Figure 5). Smoothing is a common feature of reconstructions that incorporate time uncertainty (Anchukaitis and Tierney, 2013; Bakke et al., 2013).

Because including age uncertainty inevitably smoothes the median estimate compared with any single ensemble member, the

median estimate underestimates the amplitude of temperature changes through time. The extent to which the median series (Figure 5a) is smoother can be seen by comparison with a single estimate of the 3-year-mean reconstruction that was calculated using just the best-estimate *clam* age model and the median of the regression parameters (Figure 5b). This estimate is based on the 20CR-calibrated reconstruction, which exhibits somewhat higher-amplitude fluctuations compared with the GISTEMP-based calibration.

The calibrations using the two reanalysis products (excluding HadCRUT4, which is poorly correlated with RABD) result in reconstructions with different amplitudes of inferred temperature changes (Figure 6). Over the calibration period (AD 1870–2010), temperatures in 20CR vary by more than 7°C, whereas GISTEMP shows less than 5°C of variability. Consequently, the median temperature reconstruction using the 20CR target shows a larger range of temperatures (about 9°C corresponding to RABD minima and maxima) than does the GISTEMP-based reconstruction (range=6°C). The above-freezing-days reconstruction implies considerable variability in the length of the melt season since 5.7ka, with the median estimates ranging from about 100–150 days above freezing per year (Figure 7a).

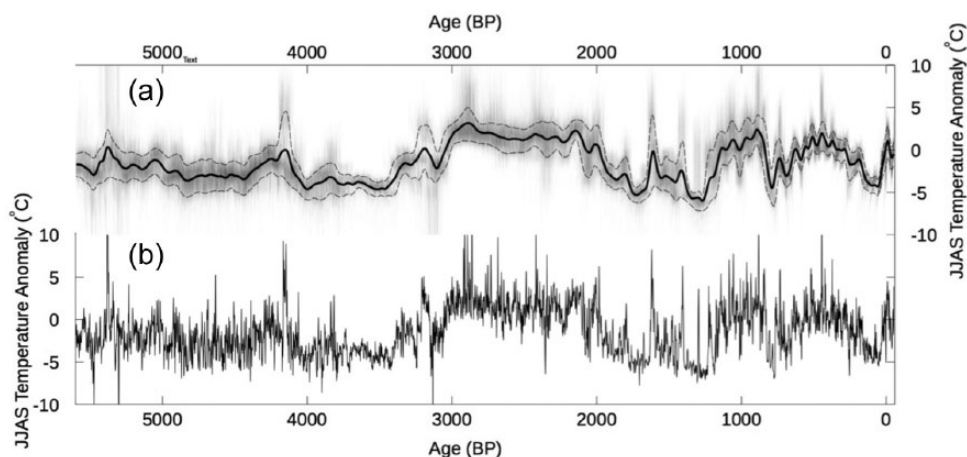


Figure 5. Chlorophyll-inferred reconstructed summer (JJAS) temperature anomalies (relative to 1961–1990) for Kurupa Lake using the 20th Century Reanalysis Project calibration (based on data shown in Figure 4 top row). (a) Weighted mean of the probability distribution for each 3-year bin (black line) and the smoothed 1σ range (dashed lines). Gray shading represents individual ensemble members, with the combined effects of age and calibration uncertainties. The weighted mean provides the best estimate of 3-year-mean temperature. (b) One reconstruction calculated using the best-estimate age model and the median regression parameters.

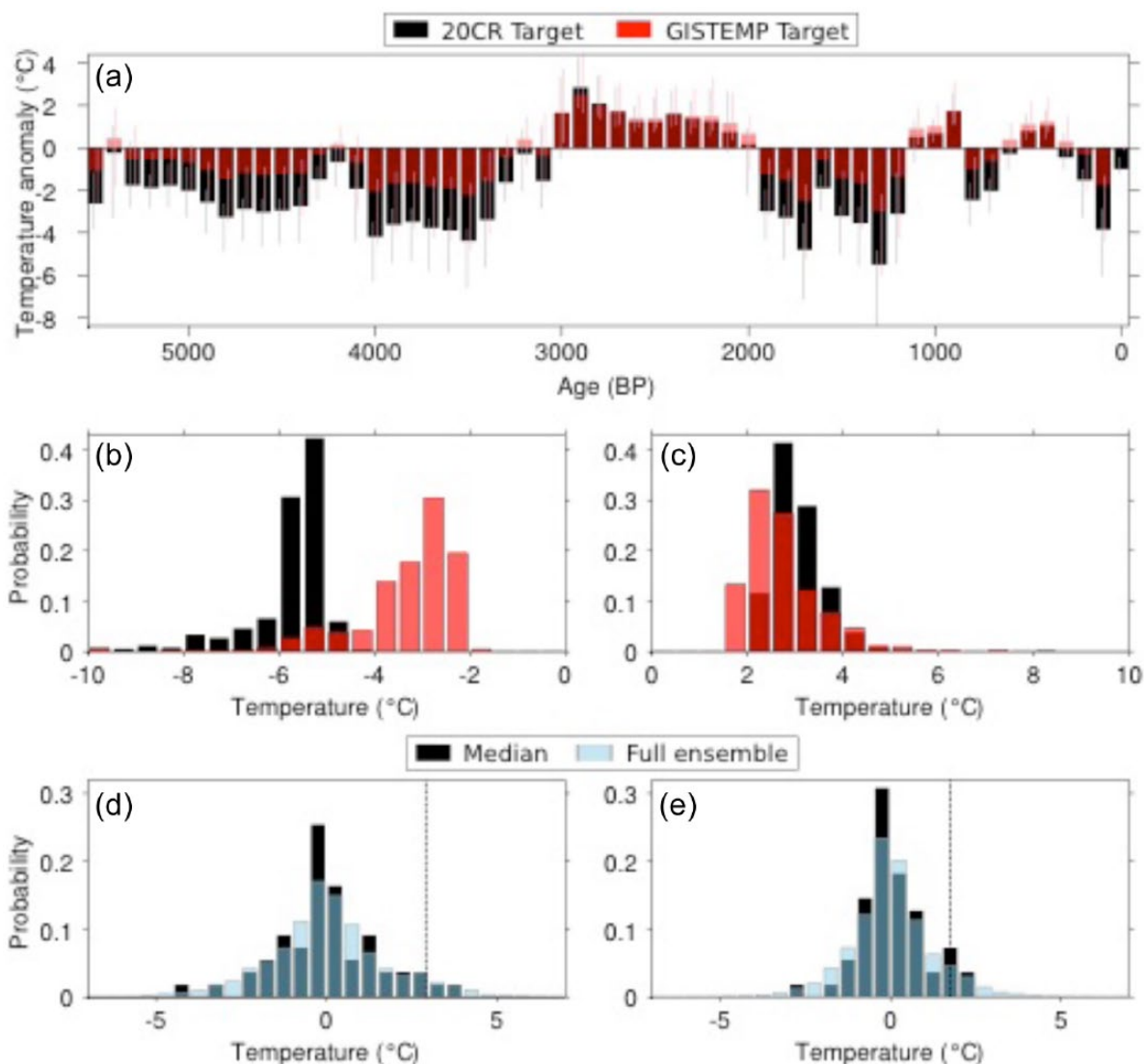


Figure 6. Centennial-mean 3-year summer temperature anomalies (relative to 1961–1990) from Kurupa Lake. (a) Median (bars) and 2σ ranges (gray and pink lines) of ensembles that incorporate the effects of age and calibration uncertainties, in addition to results based on two instrumental targets (black = 20th Century Reanalysis Project (20CR; Compo et al., 2011); red = GISTEMP (Hansen et al., 2010)). Probability distributions of the mean temperature anomaly of the (b) coldest and (c) warmest centuries over the past 5700 years, based on two instrumental targets, with colors as in (a). Distribution of century-to-century mean temperature changes based on both a single reconstruction (median of the ensemble) and the full-ensemble reconstruction for both the (d) 20CR and (e) GISTEMP targets. Vertical dashed line marks the warming between the 19th and 20th centuries, which is higher than the 90th percentile of all representations of the reconstruction.

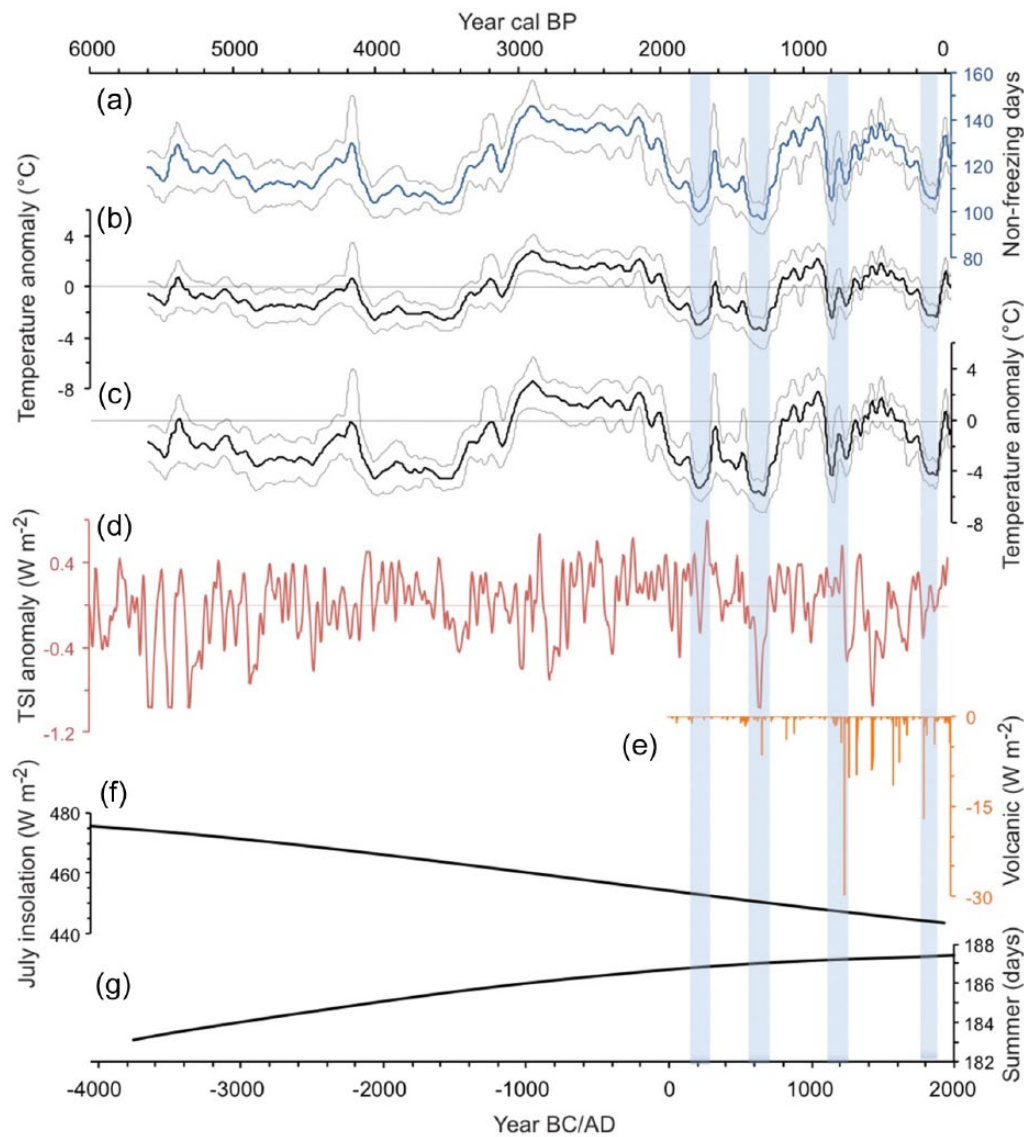


Figure 7. Kurupa Lake climate reconstructions (a)–(c) and climate-forcing mechanisms (d)–(g). Uncertainty bands in the climate reconstructions integrate age and calibration uncertainties at the 1σ range and the bands were smoothed (see Figure S1 for 2σ ranges, available online). (a) Number of non-freezing-days per year. (b) Summer (JJAS) temperature based on the calibration using the GISTEMP reanalysis product (Hansen et al., 2010). (c) Same as (b) but for the 20th Century Reanalysis Project dataset (Compo et al., 2011). (d) Total solar irradiance (TSI) relative to a mean of zero (Steinhilber et al., 2009). (e) Global volcanic forcing (Goosse et al., 2005). (f) July insolation at 65° N (Berger and Loutre, 1991). (g) Summer duration (<http://www.sym454.org/seasons/>). Vertical blue bands highlight cold intervals in the Kurupa Lake temperature reconstruction during the last 2000 years.

We focus on some key metrics of the temperature reconstruction that should be useful for comparison with climate-model output. These include the best-estimate temperature of the warmest and coldest centuries and the rates of temperature change among consecutive centuries. The median of the ensemble members is the best estimate of 3-year-mean temperature, and the scatter among ensemble members can be used to quantify reasonable uncertainties (Figure 6b and c). Using the 20CR target, the mean temperature of the warmest century (3.0–2.9 ka BP) was about 3.0°C higher (90% range of the ensemble members = 2.3°C to 4.0°C) than during the reference period (AD 1961–1990), whereas the coldest century (1.4–1.3 ka BP) was about 5.5°C lower (90% range = –7.6°C to –5.0°C) than the reference period. Using the calibration based on the lower-amplitude GISTEMP target implies temperature anomalies of 2.6 (1.8–4.2)°C and –3.0 (–5.5 to –2.3)°C for the warmest and coldest centuries, respectively. The temperature difference between consecutive centuries is approximately normally distributed

around 0°C (Figure 6d and e). The shift between the 19th and 20th centuries was 2.8 (1.9–5.1)°C and 1.8 (1.3–3.9)°C based on the 20CR and GISTEMP targets, respectively. This is above the 90th percentile of century-to-century temperature changes across all representations of the reconstruction.

The chlorophyll-inferred summer temperature and non-freezing days reconstructions from Kurupa Lake show no first-order trend over the entire 5.7 ka record (e.g. $r^2=0.04$, $p=0.41$ for linear regression over the 20CR-based temperature reconstruction). Instead, temperatures during the first half of the record, from 5.7 to 3.1 ka, were generally lower than during the second half. The longest sustained warm interval occurred during the millennium between 3 and 2 ka. Following this warm period, reconstructed summer temperature reached a minimum around AD 250 and again around AD 650. Subsequent cold phases occurred from around AD 1200–1300 and AD 1800–1900, whereas warmth prevailed from AD 900–1100, AD 1400–1600 and AD 1950 through to the present.

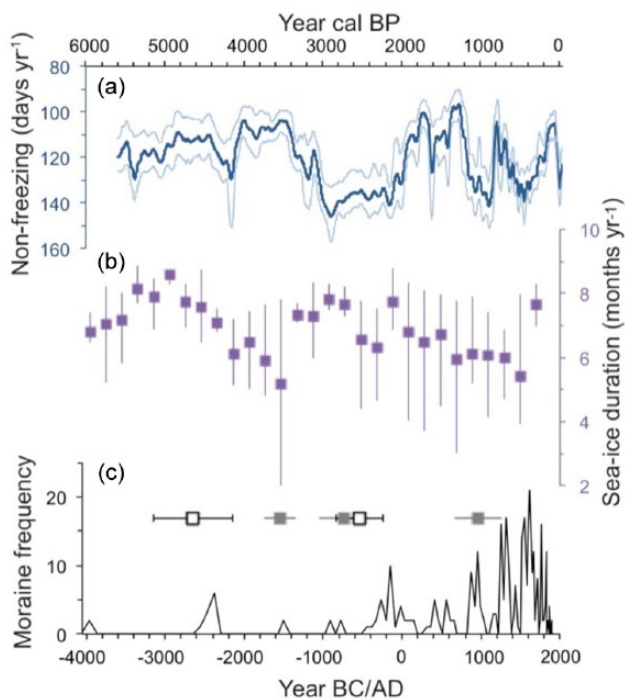


Figure 8. (a) Annual number of non-freezing days reconstructed at Kurupa Lake compared with the (b) duration of sea ice over the Chukchi Sea, and (c) frequency of Holocene moraines in the Brooks Range. The y-axes are all oriented so that colder is up. (b) The reconstruction of the sea-ice duration (months per year with >50% concentration) is the mean and range (purple squares and lines; simplified box and whisker plot) of three dinocyst-based records, each binned at 200-year intervals (GGC-19, P1/B3, and HLY0501, as summarized by de Vernal et al., 2013). (c) The frequency of moraines is based on the lichenometric-dated moraines of Ellis and Calkin (1984) and updated using the growth curve of Sikorski et al. (2009). The open and gray boxes show the mean ages (with 1σ ranges) of multiple moraines in the central Brooks Range based on ^{10}Be dating by Badding et al. (2013) and Pendleton et al. (in review), respectively.

Long-term trend: Influence of summer duration and sea ice

The lack of overall cooling in the Kurupa Lake reconstruction contrasts with most records of Arctic temperature for the past 2000 years (McKay and Kaufman, 2014; PAGES 2k Consortium, 2013), and for the Holocene-long trend at northern high latitudes (Marcott et al., 2013). The lack of millennial-scale cooling is unexpected because the precession of the equinox caused summer insolation at northern high latitudes to decrease over this period (Berger and Loutre, 1991; Figure 7f). The lack of cooling might be attributed to the counter-balancing effect of increasing summer duration on photosynthetic pigment production within Kurupa Lake (Figure 7g). While solar intensity on 21 June (and average summer insolation) decreased over the past 10 ka as the Northern Hemisphere summer solstice shifted from the perihelion to the aphelion, the orbital duration of summer, defined as the length of time between vernal and autumnal equinox, increased by 4.3 days during the past 6 ka (<http://www.sym454.org/seasons/>).

The important influence of the duration of the ice-free season on production in and around Kurupa Lake is also indicated during the instrumental period. Between 1871 and 2003, the correlation between RABD and early summer (June) plus late summer (September) temperature is slightly stronger ($r=0.74$, $p=0.02$) than the correlation with mid-summer (July + August) temperature ($r=0.66$, $p=0.03$ for the 20CR dataset). This indicates that the temperature of the transitional months has a stronger influence on

chlorophyll content in Kurupa Lake sediments than does the temperature of the warmest months.

The lack of millennial cooling at Kurupa Lake is also consistent with Holocene-long records of sea-ice cover over the Chukchi Sea (Figure 8). A recent summary based on dinocyst assemblages at three sites (de Vernal et al., 2013; Figure 1a) shows no millennial-scale change (or possibly a slight decrease) in the number of months with sea-ice concentration >50% since 8 ka. Although summer sea-ice cover is known to influence air temperatures over onshore areas (Ogi and Wallace, 2007), the sea-ice reconstruction has little resemblance to the nonfreezing-days reconstruction at Kurupa Lake. Over the longer term, however, both reconstructions show no cooling trend.

Solar and volcanic forcing

Some of the major shifts in summer temperature at Kurupa Lake seem to roughly correspond with external climate forcing (Figure 7). Centennial-scale periods of cooling around AD 650, 1250, and 1800 correspond with ice-core records of sulfate aerosols related to volcanic events (Goosse et al., 2005). Although the climate-altering impact of individual eruptions is brief, repeated large eruptions combined with feedbacks involving high-latitude sea-ice extent can lower summer temperatures for centuries, as has been inferred for the rapid glacierization on Baffin Island in the late 13th century (Miller et al., 2012).

In addition to volcanic aerosols, changes in solar output have been related to cooling events (Steinhilber et al., 2009; Wiles et al., 2004). Chlorophyll content of Kurupa Lake sediment and reconstructed total solar irradiation (TSI) do not correlate ($r=-0.04$, $p=0.72$) over the past 5.7 ka, although reconstructed TSI and volcanic activity are generally correlated, and the largest cooling event at Kurupa Lake coincides with the largest TSI minimum centered on AD 650. Although the relation is weak, changes in solar output might influence primary production at Kurupa Lake, as has been inferred for other lakes, including Arolik Lake in southwest Alaska (Hu et al., 2003).

Comparison with glacial and other records from northern Alaska

The geomorphic evidence for glacier fluctuations in the Brooks Range shows some similarities with the Kurupa Lake temperature reconstruction (Figure 8). The most extensive survey of moraines in the Brooks Range used lichenometry to infer moraine ages (Ellis and Calkin, 1984; Sikorski et al., 2009; Solomina and Calkin, 2003). Since then, Badding et al. (2013) and Pendleton et al. (in preparation) have dated Neoglacial terminal moraines in four valleys in the central Brooks Range using ^{10}Be exposure dating, and found major modes of moraine stabilization at ~ 4.6 , ~ 3.5 , and ~ 2.6 ka. The ^{10}Be chronology generally supports the ages based on lichenometry used in earlier research, and confirms that at least some Brooks Range glaciers achieved their Neoglacial maxima as early as the middle Holocene, followed by advances of similar or more limited extent. Glaciers in two of the four studied valleys reached their Neoglacial maxima at ~ 5 and 3 ka, when cold conditions prevailed at Kurupa Lake. On the other hand, ^{10}Be ages from two valleys and lichen ages from elsewhere in the Brooks Range indicate that moraines were constructed during the warm interval from 3.0 to 2.1 ka. The highest frequency of moraine ages falls within the past millennium. Modes centered around AD 1300 and 1800 generally coincide with the two prominent cold intervals in the Kurupa Lake record, whereas the mode in moraine frequency centered on AD 1600 coincides with a warm interval at Kurupa Lake. Disagreement between summer temperature and the glacial-geomorphic record implicates the

important influence of winter accumulation on glacier mass balance in the Brooks Range.

Previous research has identified asynchronicity in Holocene climate changes between the north and south sides of the Brooks Range. Mann et al. (2002) found an antiphase relation between the expansion of the Kobuk dune field (south Brooks Range) and Ikpikik dune field (north Brooks Range), and no comprehensible correlation with northern Brooks Range glacier fluctuations. In contrast, Galloway and Carter (1993) reported episodes of dune building, contemporaneous with cirque glacier advances before 4.3, 3.9–2.7, 2.0–1.1, and 0.7 ka. The Kurupa Lake record also shows asynchronous change compared with southern Brooks Range records. For example, fluctuations in chlorophyll content at Kurupa Lake do not correlate with 2000-year-long varve-inferred summer temperature at Blue Lake, Alaska (Bird et al., 2009), and the two records appear antiphased during some intervals. Similarly, the *Chara*-stem encrustation $\delta^{18}\text{O}$ record from Tangled-Up Lake (Anderson et al., 2001) does not show significant correspondence with the Kurupa Lake chlorophyll-inferred temperature reconstruction, although the records appear to be systematically offset by ~200 years ($r=0.50$, $p=0.11$ when the age of the $\delta^{18}\text{O}$ record is increased by 200 years). A recent 900-year-long tree-ring-based summer temperature reconstruction from northeastern-most Alaska (Anchukaitis et al., 2013) shows remarkable similarity in multi-decadal-scale variability, but lacks the multi-centennial low frequency, compared with the Kurupa Lake temperature reconstruction.

Conclusion

The 5700-year-long summer temperature reconstruction from Kurupa Lake shows pronounced centennial-scale variability. Nearly the entire range of downcore variability in RABD (inferred sedimentary chlorophyll content) is represented during the 20th century when instrumental records indicate that summer temperature around Kurupa Lake changed by about 5°C (based on GISTEMP; Fig. 4a) or 7°C (based on GISTEMP; Fig. 4b). The magnitude of variability in reconstructed temperature therefor reflects the pronounced variability of the calibration target, which indicates the sensitivity of the study area to changes in sea ice and Arctic amplification more generally. Using the GISTEMP dataset for calibration indicates that the average 3-year-mean temperature of the warmest century (3.0–2.9 ka BP) was about 2.6 (1.8–4.2)°C higher and the coldest century (1.4–1.3 ka BP) was about 3.0 (5.5–2.3)°C lower than the reference period (AD 1961–1990). Using the 20CR target results in temperature variability about 3°C larger than using GISTEMP, with especially pronounced cooling. Our confidence intervals for the reconstruction integrate uncertainties in both the calibration regression statistics and the age model using an ensemble approach. The median of the ensemble members is a smoothed version of the best-estimate reconstruction because it incorporates age uncertainty in estimating the median likelihood for each 3-year-temperature mean. The reconstruction is the longest quantitative temperature record with decadal resolution from Alaska. Evidence for long-term stability in Kurupa Lake gives us confidence in the inference model. Nonetheless, the chlorophyll record has not yet been replicated within Kurupa Lake or other lakes nearby, and has not been verified against other proxies.

At the millennial and finer scale, the Kurupa Lake temperature record shows little correspondence with paleoenvironmental records from northern Alaska and the Chukchi Sea. At the multi-millennial scale, the shared lack of cooling at Kurupa Lake and over the Chukchi Sea appears robust. These contrast with other Northern Hemisphere temperature reconstructions for the Holocene (Marcott et al., 2013) and at the continental scale during the

last 2000 years (PAGES 2k Consortium, 2013), which show a pervasive Holocene cooling trend. Additional proxy records are needed from the region to more confidently assess the spatial-temporal pattern of Holocene climate changes and the terrestrial impact of past sea-ice fluctuations.

Acknowledgements

We thank Mike Badding and Al Werner for assistance in the field, Katherine Whitacre, John Southon, Mike Ketterer and the staff at LacCore (University of Minnesota) for laboratory support, and R Scott Anderson and two anonymous reviewers for their insightful comments.

Funding

The research was funded by the US National Science Foundation awards ARC-1107662, ARC-1107854, and EAR-1347221.

Supplementary materials

Figure S1 and Tables S1, S2, and S3 include the raw data and age model used for the paleoclimate reconstructions, along with statistics related to the analysis of uncertainty and the reconstruction time series presented in the text.

References

- Anchukaitis KJ and Tierney JE (2013) Identifying coherent spatiotemporal modes in time-uncertain proxy paleoclimate records. *Climate Dynamics* 41: 1291–1306.
- Anchukaitis KJ, D'Arrigo RD, Andreu-Hayles L et al. (2013) Tree-ring-reconstructed summer temperatures from north-west North America during the last nine centuries. *Journal of Climate* 26: 3001–3012.
- Anderson L, Abbott MB and Finney BP (2001) Holocene climate inferred from oxygen isotope ratios in lake sediments, central Brooks Range, Alaska. *Quaternary Research* 55: 313–321.
- Anderson PM and Brubaker LB (1994) Vegetation history of north central Alaska: A mapped summary of late-Quaternary pollen data. *Quaternary Science Reviews* 13: 71–92.
- Badding ME, Briner JP and Kaufman DS (2013) ^{10}Be ages of late Pleistocene deglaciation and neoglaciation in the north-central Brooks Range, Arctic Alaska. *Journal of Quaternary Sciences* 28: 95–102.
- Bakke J, Trachsel M, Kvisvik BC et al. (2013) Numerical analyses of a multi-proxy data set from a distal glacier-fed lake, Sørsendalsvatn, western Norway. *Quaternary Science Reviews* 73: 1–14.
- Berger A and Loutre MF (1991) Insolation values for the climate of the last 10 million years. *Quaternary Sciences Reviews* 10: 297–317.
- Bird BW, Abbott MB, Finney BP et al. (2009) A 2000 year varve-based climate record from the central Brooks Range, Alaska; Late Holocene climate and environmental change inferred from Arctic lake sediment. *Journal of Paleolimnology* 41: 25–41.
- Blaauw M (2010) Methods and code for 'classical' age-modelling of radiocarbon sequences. *Quaternary Geochronology* 5: 512–518.
- Boldt BR (2013) *A multi-proxy approach to reconstructing Holocene climate variability at Kurupa River valley, Arctic Alaska*. Master's Thesis, Northern Arizona University, 114 pp.
- Bretherton S, Widmann M, Dymnikov VP et al. (1999) The effective number of spatial degrees of freedom of a time-varying field. *Journal of Climate* 12: 1990–2009.
- Compo GP, Whitaker JS, Sardeshmukh PD et al. (2011) *The twentieth century reanalysis project*. Agencies and Staff of the U.S. Department of Commerce, Paper 254. Available at: <http://digitalcommons.unl.edu/usdeptcommercepub/254>.

- Das B, Vinebrooke RD, Sanchez-Azofeifa A et al. (2005) Inferring sedimentary chlorophyll concentrations with reflectance spectroscopy: A novel approach to reconstructing historical changes in the trophic status of mountain lakes. *Canadian Journal of Fisheries and Aquatic Science* 62: 1067–1078.
- de Vernal A, Hillaire-Marcel C, Rochon A et al. (2013) Dinocyst-based reconstructions of sea ice cover concentration during the Holocene in the Arctic Ocean, the northern North Atlantic Ocean and its adjacent seas. *Quaternary Science Reviews* 79: 111–121.
- Ellis JM and Calkin PE (1984) Chronology of Holocene glaciation, central Brooks Range, Alaska. *Geological Society of America Bulletin* 95: 897–912.
- Galloway JP and Carter LD (1993) Late Holocene longitudinal and parabolic dunes in northern Alaska: Preliminary interpretations of age and paleoclimatic significance. *United States Geological Survey Bulletin* 2068: 3–11.
- Goosse H, Crowley TJ, Zorita E et al. (2005) Modelling the climate of the last millennium: What causes the differences between simulations? *Geophysical Research Letters* 32: L06710.
- Hansen J, Ruedy R, Sato M et al. (2010) Global surface temperature change. *Reviews of Geophysics* 48: RG4004.
- Hu FS, Kaufman D, Yoneji S et al. (2003) Cyclic variation and solar forcing of Holocene climate in the Alaskan subarctic. *Science* 301: 1890–1892.
- Ketterer ME, Hafer KM, Jones VJ et al. (2004) Rapid dating of recent sediments in Loch Ness: Inductively coupled plasma mass spectrometric measurements of global fallout plutonium. *Science of the Total Environment* 322: 221–229.
- Lynch AH, Slater AG and Serreze M (2001) The Alaskan Arctic frontal zone: Forcing by orography, coastal contrast, and the boreal forest. *Journal of Climate* 14: 4351–4362.
- McKay NP and Kaufman DS (2014) An extended Arctic proxy temperature database for the past 2,000 years. *Scientific Data* 1: 140026.
- Mann DH, Heiser PA and Finney BP (2002) Holocene history of the Great Kobuk sand dunes, northwestern Alaska. *Quaternary Science Reviews* 21: 709–731.
- Marcott SA, Shakun JD, Clark PU et al. (2013) A reconstruction of regional and global temperature for the past 11,300 years. *Science* 339: 1198–1201.
- Michelutti N, Blais JM, Cumming BF et al. (2010) Do spectrally inferred determinations of chlorophyll a reflect trends in lake trophic status? *Journal of Paleolimnology* 43: 205–217.
- Michelutti N, Wolfe AP, Vinebrooke RD et al. (2005) Recent primary production increases in arctic lakes. *Geophysical Research Letters* 32: L19715.
- Miller GH, Geirsdóttir Á, Zhong Y et al. (2012) Abrupt onset of the Little Ice Age triggered by volcanism and sustained by sea-ice/ocean feedbacks. *Geophysical Research Letters* 39: L02708.
- Morice CP, Kennedy JJ, Rayner NA et al. (2012) Quantifying uncertainties in global and regional temperature change using an ensemble of observational estimates: The HadCRUT4 dataset. *Journal of Geophysical Research* 117: D08101.
- Ogi M and Wallace JM (2007) Summer minimum Arctic sea ice extent and the associated summer atmospheric circulation. *Geophysical Research Letters* 34: L12705.
- PAGES 2k Consortium (2013) Continental-scale temperature variability during the past two millennia. *Nature Geoscience* 6: 339–346.
- Pendleton SL, Ceperley EG, Briner JP et al. (in review) Rapid and early deglaciation of the central Brooks Range, Arctic Alaska. *Geology*.
- Polyak L, Alley RB, Andrews JT et al. (2010) History of sea ice in the Arctic. *Quaternary Science Reviews* 29: 1757–1778.
- Rein B and Sirocko F (2002) In-situ reflectance spectroscopy-analysing techniques for high-resolution pigment logging in sediment cores. *International Journal of Earth Sciences* 91: 950–954.
- Saunders KM, Grosjean M, Hodgson DA (2013) A 950 yr temperature reconstruction from Duckhole Lake, southern Tasmania, Australia. *The Holocene* 23: 771–783.
- Sikorski JJ, Kaufman DS, Manley WF et al. (2009) Glacial-geological evidence for decreased precipitation during the Little Ice Age in the Brooks Range, Alaska. *Arctic, Antarctic, and Alpine Research* 41: 138–150.
- Smol JP (1988) Paleoclimatic proxy data from freshwater Arctic diatoms. *Verhandlungen der Internationalen Verein für Limnologie* 23: 37–44.
- Solomina O and Calkin PE (2003) Lichenometry as applied to moraines in Alaska, U.S.A., and Kamchatka, Russia. *Arctic, Antarctic, and Alpine Research* 35: 129–143.
- Steinhilber F, Beer J and Fröhlich C (2009) Total solar irradiance during the Holocene. *Geophysical Research Letters* 36: L19704.
- Stone RS, Dutton EG, Harris JM et al. (2002) Earlier spring snowmelt in northern Alaska as an indicator of climate change. *Journal of Geophysical Research* 107: 1–14.
- Stuvier M, Reimer PJ and Reimer RW (2005) CALIB 5.0 (WWW program and documentation). Available at: <http://calib.qub.ac.uk/calib/>.
- Sundqvist HS, Kaufman DS, McKay NP et al. (2014) Arctic Holocene proxy climate database – New approaches to assessing geochronological accuracy and encoding climate variables. *Climate of the Past* 10: 1605–1631.
- von Gunten L, Grosjean M, Kamenik C et al. (2012) Calibrating biogeochemical and physical climate proxies from non-varved lake sediments with meteorological data: Methods and case studies. *Journal of Paleolimnology* 47: 583–600.
- von Gunten L, Grosjean M, Rein B et al. (2009) A quantitative high-resolution summer temperature reconstruction based on sedimentary pigments from Laguna Aculeo, central Chile, back to AD 850. *The Holocene* 19: 873–881.
- Walsh JE and Chapman WL (2001) 20th-century sea-ice variations from observational data. *Annals of Glaciology* 33: 444–448.
- Walsh JE, Overland JE, Groisman PY et al. (2011) Ongoing climate change in the Arctic. *Ambio* 40: 6–16.
- Wiles GC, D'Arrigo RD, Villalba R et al. (2004) Century-scale solar variability and Alaskan temperature change over the past millennium. *Geophysical Research Letters* 31: L15203.
- Wolfe AP, Vinebrooke RD, Michelutti N et al. (2006) Experimental calibration of lake-sediment spectral reflectance to chlorophyll a concentrations: Methodology and paleolimnological validation. *Journal of Paleolimnology* 36: 91–100.